NUMERICAL SIMULATIONS OF VISCOELASTIC FLOWS IN FIBROUS POROUS MEDIA

H. L. Liu and W. R. Hwang*
School of Mechanical Engineering, Gyeongsang National University, Jinju, South Korea
* Corresponding author (wrhwang@gnu.ac.kr)

Keywords: *viscoelastic flow, porous media, flow resistance, resin transfer molding*

1 Introduction

Viscoelastic flow in porous media has important applications in engineering fields such as composite manufacturing, textile coating and chemical enhanced oil recovery industry. The flow resistance of polymeric surfactant in porous system is of great interest. Experimental results [1-4] indicate a gradually increment dramatic increase of flow resistance above a critical Weissenberg number. However, the steady state numerical simulations show that no evident increase of flow resistance with increasing pure elasticity [5-8]. Talwar and Khomami [9] simulated creeping flow of shear thinning viscoelastic fluids past periodic regular arrays of fibers with different viscoelastic models and their results indicated that as the pressure drop is progressively increased, the flow resistance decreases initially and then rebounds to its initial value. These discrepancies between their works motivate current numerical study to investigate effects of elasticity, shear-thinning and elongational hardening of a fluid on the flow resistance to the porous system.

In this work, we present a numerical simulation of various viscoelastic fluids in fibrous porous media to investigate effects of elasticity and shear-thinning on the flow resistance. We employ the DEVSS/DG finite element scheme combined with the mortar-element method for the bi-periodic boundary condition and the fictitious domain method for fibers in a fluid. The matrix logarithm has been incorporated in our numerical scheme to achieve a stable solution at high Weissenberg number. By employing Oldroyd-B and Leonov models as constitutive equations, we discuss effects of elasticity and shear-thinning of viscoelastic flow on the flow resistance in various uni-directional fibrous porous microstructures.

2 Modeling

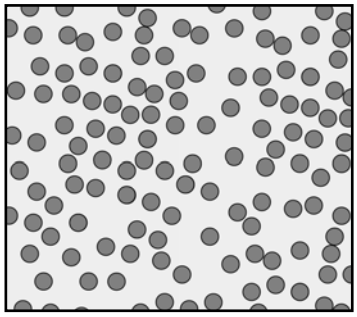

Fig. 1. Example of cross sectional microstructure of random packing unidirectional fibers.

In this work, the transversal flow crossing a porous media is modeled as the flow through the unidirectional cylinders. Fig. 1 is the schematic description of cross section of our porous system with many random packing fibers. A fictitious domain method [10, 11] has been implemented to describe the solid cylinder. In this method, the cylinder is considered as an immobilized rigid ring, which is filled with the same fluid as in the fluid domain and the zero velocity condition is imposed only along the fiber boundary.

The set of government equations is given by:

$$\nabla \cdot \boldsymbol{u} = 0 \tag{1}$$

$$\nabla \cdot \boldsymbol{\sigma} = \mathbf{0} \tag{2}$$

$$\boldsymbol{\sigma} = -p\boldsymbol{I} + 2\eta_s \boldsymbol{D} + \boldsymbol{\tau}_p \tag{3}$$

Eqs. (1)-(3) are equations for the momentum balance, the continuity, the constitutive relation. The

constitutive relations of employed viscoelastic models are given as:

$$\lambda \overset{\nabla}{\boldsymbol{\tau}}_p + \boldsymbol{\tau}_p - 2\eta_p \boldsymbol{D} = 0, \tag{4}$$

$$\overset{\nabla}{\boldsymbol{\tau}}_p + \frac{1}{\lambda}\boldsymbol{\tau}_p - \frac{1}{2G\lambda}\boldsymbol{\tau}_p \cdot \boldsymbol{\tau}_p = 2G\boldsymbol{D}, \tag{5}$$

$$\overset{\nabla}{\boldsymbol{\tau}}_p \equiv \frac{\partial \boldsymbol{\tau}_p}{\partial t} + \boldsymbol{u}\cdot\nabla\boldsymbol{\tau}_p - \left(\nabla \boldsymbol{u}\right)^T \cdot \boldsymbol{\tau}_p - \boldsymbol{\tau}_p \cdot \nabla \boldsymbol{u}. \tag{6}$$

Eqs. (4) and (5) are Oldroyd-B and Leonov models as constitutive equations and symbol ' ∇ ' denotes the upper-convected time derivative which is define by Eq. (6). Following previous works [7-9], the corrected flow resistance coefficient which only represents the effect of elasticity is the ratio of flow rates in porous media between the corresponding inelastic viscous and viscoelastic flows as:

$$fRe_{corr.} = \frac{Q_{viscous}}{Q_{viscoelastic}}. \tag{7}$$

The Carreau-Yasuda model, including a Newtonian solvent viscosity η_s, is employed to describe the inelastic non-Newtonian flow as:

$$\eta_{cy} = \eta_s + \frac{\eta_0}{\left[1+\left(\lambda\dot{\gamma}\right)^a\right]^{(1-n)/a}} \tag{8}$$

Furthermore, the Weissenberg number is defined by:

$$We = \lambda Q / L^2 \tag{9}$$

where λ is the relaxation time of viscoelastic fluid , Q is the flow rate and L represents the characteristic length of interstice in porous microstructure.

4. Numerical methods

We employ the DEVSS scheme which is a mixed finite-element method together with the Matrix Logarithms for accurate and stable computation of viscoelastic flow to a relative high Weissenberg number. The DG formulation is used for the discretization of the viscoelastic constitutive equation. For the combination of the DEVSS formulation, we introduce an extra variable $\boldsymbol{e}$, the viscous polymer stress.

$$\boldsymbol{e} = 2\eta_p \boldsymbol{D} \tag{10}$$

We introduced three different Lagrangian multipliers $\boldsymbol{\lambda}^{\mathrm{B},i}$, $\boldsymbol{\lambda}^{\mathrm{h}}$ and $\boldsymbol{\lambda}^{\mathrm{v}}$, which are associated with the rigid-ring constraint along the $i-th$ fiber, kinematic constrains for periodicity in horizontal and vertical directions. The weak form for the whole domain can be stated as:

Find $\left(\boldsymbol{u}, p, \boldsymbol{\tau}_p, \boldsymbol{e}, \boldsymbol{\lambda}^{\mathrm{B},i}, \boldsymbol{\lambda}^{\mathrm{h}}, \boldsymbol{\lambda}^{\mathrm{v}}\right)$ such that

$$-\int_\Omega p\nabla\cdot v\, d\Omega + \int_\Omega \boldsymbol{D}[\boldsymbol{v}] : 2\eta_0 \boldsymbol{D}[\boldsymbol{u}]\, d\Omega - \int_\Omega \boldsymbol{e} : \boldsymbol{D}[\boldsymbol{v}]\, d\Omega$$
$$+\sum_{i=1}^{N}(\boldsymbol{\lambda}^{\mathrm{B},i}, \boldsymbol{v}) + \left(\boldsymbol{\lambda}^{\mathrm{h}}, \boldsymbol{v}(0,y) - \boldsymbol{v}(L,y)\right)_{\Gamma_4},$$
$$+\left(\boldsymbol{\lambda}^{\mathrm{v}}, \boldsymbol{v}(x,H) - \boldsymbol{v}(x,0)\right)_{\Gamma_3} = \int_\Omega \boldsymbol{\tau}_p : \boldsymbol{D}[\boldsymbol{v}]\, d\Omega, \tag{11}$$

$$\int_\Omega q\nabla\cdot v\, d\Omega = 0, \tag{12}$$

$$-\int_\Omega \boldsymbol{e}_s : \boldsymbol{D}(\boldsymbol{u})\, d\Omega + \frac{1}{2\eta_p}\int_\Omega \boldsymbol{e}_s : \boldsymbol{e}\, d\Omega = 0, \tag{13}$$

$$\int_\Omega \boldsymbol{S} : \left(\lambda \overset{\nabla}{\boldsymbol{\tau}}_p + \boldsymbol{\tau}_p - 2\eta_p \boldsymbol{D}\right) d\Omega$$
$$-\lambda\sum_{e=1}^{nel}\int_{\Gamma_e^{in}} \boldsymbol{S} : \left(\boldsymbol{\tau}_p - \boldsymbol{\tau}_p^{\mathbf{ext}}\right)(\boldsymbol{u}\cdot\boldsymbol{n})\, d\Gamma = 0, \tag{14}$$

$$(\boldsymbol{\mu}^{\mathrm{B},i}, \boldsymbol{u}) = 0,\ (i = 1,...,N) \tag{15}$$

$$\left(\boldsymbol{\mu}^{\mathrm{h}}, \boldsymbol{u}(0,y) - \boldsymbol{u}(L,y)\right)_{\Gamma_4} = 0, \tag{16}$$

$$\left(\boldsymbol{\mu}^{\mathrm{v}}, \boldsymbol{u}(x,H) - \boldsymbol{u}(x,0)\right)_{\Gamma_3} = 0, \tag{17}$$

for all $\left(\boldsymbol{v}, q, \boldsymbol{S}, \boldsymbol{e}_s, \boldsymbol{\mu}^{\mathrm{B},i}, \boldsymbol{\mu}^{\mathrm{h}}, \boldsymbol{\mu}^{\mathrm{v}}\right)$.

For the discretization of the weak form, we employ the regular quadrilateral elements with continuous bi-quadratic interpolation for the velocity $\boldsymbol{u}$, discontinuous linear interpolation for the pressure p, continuous bi-linear interpolation for the viscous polymer stress $\boldsymbol{e}$ and discontinuous bi-linear interpolation for the polymer stress $\boldsymbol{\tau}_p$. The polymer stress tensor is treated by a matrix logarithmic formulation and thus the stable solution to high Weissenberg number has been achieved [12].

After implementing above discretization, one gets a sparse matrix with non-zeros off the diagonal. A direct solver (HSL2002/MA41) based on the sparse

multi-frontal variant of Gaussian elimination is used to solve the final matrix.

3 Results and discussion

We performed the mesh refinement test for the Oldroyd-B fluid with a cylinder in the center of a square domain. The radius of the fiber is 0.2 and the size of domain is 1×1. We used three different meshes of 25×25, 50×50 and 100×100 elements, which are denoted by M1, M2 and M3, respectively. The trace of conformation tensor along the center line $(x = 0.5)$ under three different meshes M1, M2 and M3 are presented in Fig. 2 and indicate good convergence in the mesh refinement. In addition, we checked the introduction of the matrix logarithm and the result shows that the implement of matrix logarithm eliminates the instable oscillation around the interface between the fiber and viscoelastic fluid.

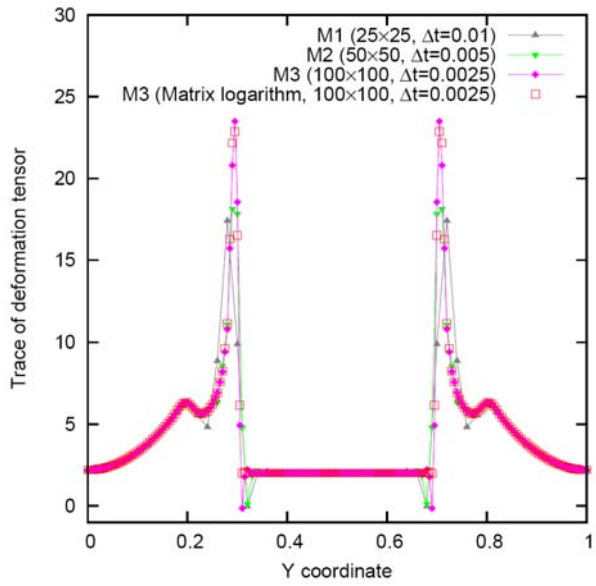

Fig. 2. The mesh convergence test for the Oldroyd-B fluid past a cylinder with three different meshes, as well as the comparison with the implement of the matrix logarithm.

Having validated our numerical scheme, we compare our simulation of Oldroyd-B fluid with previous experimental and numerical studies for the problem involved flows of Boger fluids through square array of motionless cylinders [2, 8]. The simulation conditions are fitted to the experiments done by Skartsis et al. [2]. The numerically determined flow resistance is presented as a function of Weissenberg number in Fig. 3. The previous numerical results by UCM and Oldroyd-B models have also been reproduced along with our results. The experiment data manifest a dramatic increase of flow resistance above a critical Weissenberg number $(We = 0.25)$, however the numerical predictions by Talwar and Khomami [8] for both models indicate a steady decline of fluid resistance with the restriction to Weissenberg number at about $We = 5$. In contrast to their numerical results, our computation show a slight increase of flow resistance until $We = 20$.

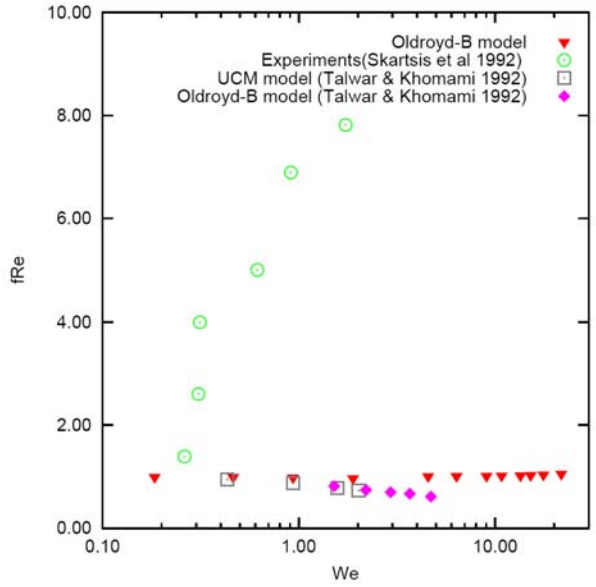

Fig. 3. The flow resistance predictions by Oldroyed-B model in a square packing fiber array with the comparison with earlier experimental data [2] and numerical study [8].

In order to understand the effect of fiber configuration on flow resistance, we performance the flow simulation by both Oldroyd-B and Leonov models in 100 random packing fibers as depicted in Fig. 1. The numerical predicted flow resistance in 100 random packing fibers shows a dramatic increase of flow resistance with respect to Weissenberg number by Oldroyed-B model as plotted in Fig. 4. Furthermore, the corrected friction coefficient for Leonov model, which only reflect the elasticity effects on flow resistance by exclusion the shear thinning effect, also exhibits the steady increase. For the case of square packing fibers, the

Oldroyed-B and Leonov models indicates only a slight increase of corrected flow resistance. The mechanism which leads to the evident increase of flow resistance in random packing fibers need to be further investigated.

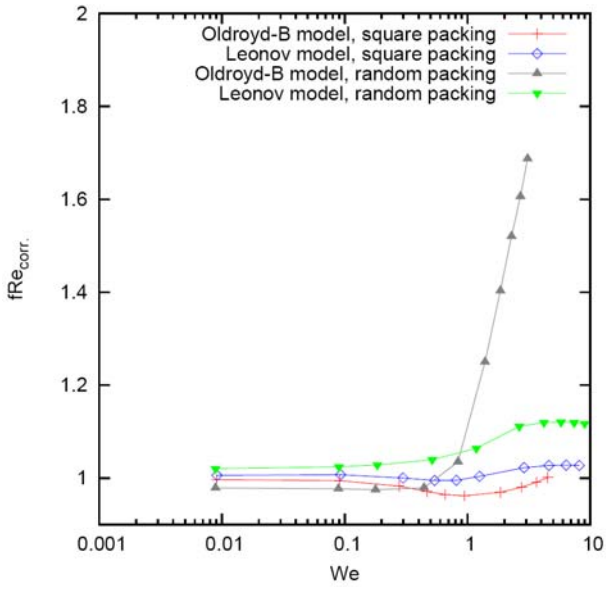

Fig. 4. The corrected flow resistance predictions by Oldroyd-B and Leonov models in square and random packing fiber arrays.

4. Conclusions

We present a numerical simulation of various viscoelastic fluids in fibrous porous media to investigate effects of elasticity and shear-thinning on the flow resistance. We employ the DEVSS/DG finite element scheme combined with the mortar-element method for the bi-periodic boundary condition and the fictitious domain method for fibers in a fluid. The matrix logarithm has been incorporated in our numerical scheme to achieve a stable solution at high Weissenberg number. The dramatic increase of flow resistance has been observed in random packing structures at high Weissenberg number.

Acknowledgements

This work is supported by the National Research Foundation of Korea (NRF) funded by the Ministry of Education, Science and Technology (2009-0094015 and 2010-0021614).

References

[1] S. Vossoughi and F. A. Seyer, Pressure drop for flow of polymer solution in a model porous medium, The Canadian Journal of Chemical Engineering, Vol. 52 pp 666-669, 1974.

[2] L. Skartsis, B. Khomami and J. L. Kardos, Polymeric flow through fibrous media, Journal of Rheology, Vol. 36, pp 589-620, 1992.

[3] C. Chmielewski, C. A. Petty and K. Jayaraman, Cross flow of elastic liquid through arrays of cylinders, Journal of Non-Newtonian Fluid Mechanics, Vol. 24, pp 309-325, 1990.

[4] C. Chmielewski and K. Jayaraman, The effect of polymer extensibility on crossflow of polymer solutions through cylinder arrays. Journal of Rheology, Vol. 36, pp 1105–1126, 1992.

[5] J. A. Deiber and W. R. Schowalter, Modeling the flow of viscoelastic fluids through porous media. AIChE Journal, Vol. 27, pp 912–920, 1987.

[6] A. Souvaliotis and A.N. Beris, Applications of domain decomposition spectral collocation methods in viscoelastic flows through model porous media, Journal of Rheology, Vol. 36, pp 1417-1453, 1992.

[7] A. Souvaliotis and A. N. Beris, Spectral collocation/domain decomposition method for viscoelastic flow simulations in model porous geometries, Computer Methods in Applied Mechanics and Engineering, Vol. 129, pp 9–28, 1992.

[8] K. K. Talwar and B. Khomami, Application of higher order finite element methods to viscoelastic flow in porous media, Journal of Rheology, Vol. 36, pp 1377– 1416, 1992.

[9] K. K. Talwar and B. Khomami, Flow of viscoelastic fluids past periodic square arrays of cylinders: inertial and shear thinning viscosity and elasticity effects, Journal of Non-Newtonian Fluid Mechanics, Vol. 57, 177-202, 1995.

[10] W. R. Hwang, M. A. Hulsen and H. E. H. Meijer, Direct simulation of particle suspensions in sliding bi-periodic frames, Journal of Computational Physics, Vol. 194, pp 742-772, 2004.

[11] W. R. Hwang and M. A. Hulsen, Direct numerical simulations of hard particle suspensions in planar elongational flow, Journal of Non-Newtonian Fluid Mechanics, Vol. 136, pp. 167-178, 2006.

[12] M. A. Hulsen, R. Fattal and R. Kupferman, Flow of viscoelastic fluids past a cylinder at high Weissenberg number: Stabilized simulations using matrix logarithms, Journal of Non-Newtonian Fluid Mechanics, Vol. 127, pp. 27-39, 2005.